

Landau Damping in a 2D Electron Gas with Imposed Quantum Grid

I. Kuzmenko

Department of Physics, Ben-Gurion University of the Negev, Beer-Sheva
(November 14, 2018)

Dielectric properties of semiconductor substrate with imposed two dimensional (2D) periodic grid of quantum wires or nanotubes (quantum crossbars, QCB) are studied. It is shown that a capacitive contact between QCB and semiconductor substrate does not destroy the Luttinger liquid character of the long wave QCB excitations. However, the dielectric losses of a substrate surface are drastically modified due to diffraction processes on the QCB superlattice. QCB-substrate interaction results in additional Landau damping regions of the substrate plasmons. Their existence, form and the density of losses are strongly sensitive to the QCB lattice constant.

PACS: 78.67.-n; 77.22.Gm; 73.90.+f

I. INTRODUCTION

Recently, new experimental techniques have made it possible to grow nanostructures which are topologically one-dimensional (1D), such as quantum wires and carbon nanotubes. One of the most exciting developments in this field is fabrication of 2D networks by means of self-assembling, etching, lithography and imprinting techniques.^{1,2} Arrays of interacting quantum wires may be formed in organic materials and in striped phases of doped transition metal oxides. Especially remarkable is a recent experimental proposal to fabricate 2D periodic grids from single-wall carbon nanotubes (SWCNT) suspended above a dielectric substrate.^{3,4} The possibility of exciting a SWCNT by external electric field together with its mechanical flexibility makes such a grid formed by nanotubes a good candidate for an element of random access memory for molecular computing. They are especially promising objects for studying novel electronic correlation properties, which, in particular, are relevant for tracing Luttinger liquid (LL) finger-prints in two dimensions. This challenging idea is motivated by noticing some unusual properties of electrons in Cu-O planes in High- T_c materials.⁵

A double 2D grid, i.e., two superimposed crossing arrays of parallel conducting quantum wires or nanotubes, represents a specific nano-object – quantum crossbars (QCB). Its spectral properties can not be treated in terms of purely 1D or 2D electron liquid theory. A constituent element of QCB (quantum wire or nanotube) possesses the LL-like spectrum.^{6,7} A single array of parallel quantum wires is still a LL-like system qualified as a sliding phase⁸ provided only the electrostatic interaction between adjacent wires is taken into account. If tunneling is suppressed and the two arrays are coupled only by electrostatic interaction in the crosses, the system possesses the LL zero energy fixed point, and besides, a rich Bose-type excitation spectrum (plasmon modes) arises at finite energies in the 2D Brillouin zone (BZ).^{9,10}

QCB is a unique system which possesses the properties of 1D and 2D liquid depending on the type of experimental probe. Some possibilities of observation of 1D \rightarrow 2D crossover in transport measurements were discussed in Ref.⁸ Several crossover effects such as appear-

ance of non-zero transverse space correlations and periodic energy transfer between arrays ("Rabi oscillations") were discussed in Refs.^{10–12}

The spectral peculiarities of QCB are directly manifested in its interaction with an external ac electromagnetic field or with conducting and/or dielectric substrates, whose electrodynamic properties are well known. To estimate this response one should note that two main parameters characterizing the plasmon spectrum in QCB are the Fermi velocity v of electrons in a wire and the QCB period a (we assume both periods to be equal). These parameters define both typical QCB plasmon wave numbers $k = |\mathbf{k}| \sim Q = 2\pi/a$ and typical plasmon frequencies $\omega \sim \omega_Q = vQ$. Choosing according to Refs.^{7,3} $v \approx 8 \cdot 10^7$ cm/sec and $a \approx 20$ nm, one finds that characteristic plasmon frequencies lie in far infrared region $\omega \sim 10^{14}$ sec⁻¹, while characteristic wave vectors are estimated as $q \sim 10^6$ cm⁻¹.

In this paper, QCB interaction with semiconductor substrate is studied. Any surface wave excited in the substrate is coupled with QCB-plasmon modes due to the substrate-QCB interaction. This interaction might be strong enough because surface plasmon waves exist in the same frequency and wave vector area as plasmons in QCB (see subsection II C for details). Therefore exciting the substrate plasmons one can probe the QCB characteristics. Indeed, substrate-QCB interaction substantially changes the conventional picture of substrate dielectric losses. Due to such interaction, new regions of Landau damping appear. The existence of these regions themselves, as well as their structure and the density of losses are sensitive to both QCB period a and the direction of the wave vector \mathbf{k} of the initial wave. Thus, dielectric losses in QCB-substrate system serve as a good tool for studying QCB spectral properties.

The structure of the paper is as follows. In Section II, we briefly describe double square QCB interacting with the dielectric substrate and introduce the necessary definitions. Dielectric properties of the system considered are studied in Section III, where Dyson-type equations for the polarization operator are obtained and analyzed. The detailed description of new regions of Landau damping is presented in Section IV. In Conclusion we summarize the results obtained.

II. QUANTUM CROSSBARS ON SEMICONDUCTOR SUBSTRATE

A. Quantum Crossbars

A square QCB is a 2D grid, formed by two periodically crossed perpendicular arrays of 1D quantum wires or carbon nanotubes. A single wire is characterized by its radius r_0 , length L , and LL interaction parameter g . The minimal nanotube radius is $r_0 \approx 0.35$ nm,¹³ maximal nanotube length is $L \approx 1$ mm, and the LL parameter is estimated as $g \approx 0.3$.⁷

In experimentally realizable setups³ the QCB is a cross-structure of suspended single-wall carbon nanotubes lying in two parallel planes separated by an inter-plane distance d , placed on a dielectric or semiconductor substrate (see Fig.1). Nevertheless, some generic properties of QCB may be described under the assumption that QCB is a genuine 2D system. We choose coordinate system so that 1) the axes x_j and corresponding basic unit vectors \mathbf{e}_j are oriented along the j -th array ($j = 1, 2$); 2) the x_3 axis is perpendicular to the QCB plane; 3) the x_3 coordinate is zero for the second array, $-d$ for the first one, and $-(d+D)$ for the substrate. The basic vectors of the reciprocal superlattice for a square QCB are $Q\mathbf{e}_{1,2}$, $Q = 2\pi/a$ so that an arbitrary reciprocal superlattice vector \mathbf{m} is a sum $\mathbf{m} = \mathbf{m}_1 + \mathbf{m}_2$, where $\mathbf{m}_j = m_j Q\mathbf{e}_j$ (m_j integer). An arbitrary vector $\mathbf{k} = k_1\mathbf{e}_1 + k_2\mathbf{e}_2$ of reciprocal space can be written as $\mathbf{q} + \mathbf{m}$ where \mathbf{q} belongs to the first BZ $|q_{1,2}| \leq Q/2$.

In a typical experimental setup³ the characteristic lengths mentioned above have the following values

$$d \approx 2 \text{ nm}, \quad L \approx 0.1 \text{ mm},$$

so that the inequalities

$$r_0 \ll d \ll a \ll L$$

are satisfied.

The QCB Hamiltonian,

$$H_{QCB} = H_1 + H_2 + H_{12} \quad (1)$$

consists of three terms. The first (second) of them describes LL in the first (second) array:

$$H_j = \frac{\hbar}{2} \sum_{\mathbf{q}, \mathbf{m}_j} \left\{ vg\pi_{j,\mathbf{q}+\mathbf{m}_j}^\dagger \pi_{j,\mathbf{q}+\mathbf{m}_j} + \frac{\omega_{q_j+m_j}^2}{vg} \theta_{j,\mathbf{q}+\mathbf{m}_j}^\dagger \theta_{j,\mathbf{q}+\mathbf{m}_j} \right\}, \quad j = 1, 2,$$

where (θ_j, π_j) are the conventional canonically conjugate boson fields and $\omega_k = v|k|$. The inter-array interaction,

$$H_{12} = \frac{\hbar\phi}{vg} \sum_{\mathbf{q}, \mathbf{m}} \xi_{q_1+m_1} \xi_{q_2+m_2} Q \theta_{1,\mathbf{q}+\mathbf{m}_1}^\dagger \theta_{2,\mathbf{q}+\mathbf{m}_2}, \quad (2)$$

$$\phi = \frac{gV_0 r_0^2}{\hbar v a}, \quad \xi_k = \omega_k \text{sign} k, \quad V_0 = \frac{2e^2}{d},$$

results from a short-range contact capacitive coupling in the crosses of the bars.¹² For QCB formed by carbon nanotubes, $\phi \sim 0.007$.

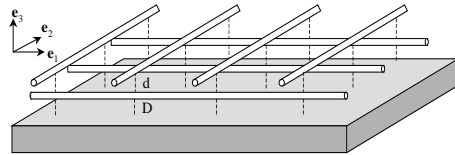


FIG. 1. QCB on a substrate. \mathbf{e}_μ ($\mu = 1, 2, 3$) are basic vectors of the coordinate system. The vector \mathbf{e}_1 (\mathbf{e}_2) is oriented along the first (second) array. The inter-array distance is d and the distance between the substrate and the first (lower) array is D .

The QCB Hamiltonian (1) describes a system of coupled harmonic oscillators, and can be diagonalized exactly. The diagonalization procedure is, nevertheless, rather cumbersome due to the mixing of states belonging to different bands and arrays. However, separability of the interaction (2) facilitates the diagonalization procedure and allows one to describe the QCB spectrum analytically.¹² Moreover, being small, this interaction grossly conserves the unperturbed 1D systematics of levels and states, at least in the low energy region corresponding to the first few energy bands. This means that perturbed eigenstates could be described in terms of the same quantum numbers (array number, band number and quasimomentum) as the unperturbed eigenstates of an “empty” lattice ($\phi = 0$).

Such a description fails in two specific regions of the reciprocal space \mathbf{k} . The first one is the vicinity of the high symmetry lines $k_j = nQ/2$ with n integer (the lines with $n = \pm 1$ include BZ boundaries). Around these lines, the *inter-band* mixing is significant and two modes from adjacent bands are degenerate. The second region is the vicinity of the resonant lines $k_1 \pm k_2 = nQ$ where the eigenfrequencies of the unperturbed plasmons

$$\omega_j(\mathbf{k}) = v|k_j|, \quad j = 1, 2,$$

from the same band propagating along two arrays coincide, $\omega_1(\mathbf{k}) = \omega_2(\mathbf{k} + \mathbf{m})$. Around resonant lines, *inter-array* mixing is significant and at these lines two modes corresponding to different arrays are degenerate. In what follows we restrict our consideration by the first BZ quarter, $0 \leq q_1, q_2 \leq Q/2$. Here the dispersion laws outside the inter-band and inter-array mixing regions conserve their unperturbed form.

B. Substrate characteristics

The substrate is described by the Hamiltonian

$$H_s = H_K + H_C, \quad (3)$$

where

$$H_K = \sum_{\mathbf{q}, \mathbf{m}} \varepsilon_{\mathbf{q}+\mathbf{m}} c_{\mathbf{q}+\mathbf{m}}^\dagger c_{\mathbf{q}+\mathbf{m}}, \quad \varepsilon_{\mathbf{k}} = \frac{\hbar^2 k^2}{2m},$$

is a kinetic energy of the substrate electrons with effective mass m and quadratic dispersion law (we omit the irrelevant spin variables), and

$$H_C = \frac{1}{2} \sum_{\mathbf{q}\mathbf{m}} U_{\mathbf{q}+\mathbf{m}} \rho_{\mathbf{q}+\mathbf{m}}^\dagger \rho_{\mathbf{q}+\mathbf{m}},$$

$$\rho_{\mathbf{k}} = \frac{1}{L} \sum_{\mathbf{k}'} c_{\mathbf{k}'}^\dagger c_{\mathbf{k}+\mathbf{k}'}, \quad U_{\mathbf{k}} = \frac{2\pi e^2}{k}, \quad \mathbf{k} = \mathbf{q} + \mathbf{m},$$

is Coulomb interaction within the substrate.

Dielectric properties of substrate *per se* are described by its dielectric function $\epsilon_s(\mathbf{k}, \omega)$,

$$\frac{1}{\epsilon_s(\mathbf{k}, \omega)} = 1 + U_{\mathbf{k}} \Pi_s(\mathbf{k}, \omega). \quad (4)$$

Within the RPA approach, the polarization operator $\Pi_s(\mathbf{k}, \omega)$ is presented by the Lindhard expression

$$(\Pi_s(\mathbf{k}, \omega))^{-1} = (\Pi_0(\mathbf{k}, \omega))^{-1} - U_{\mathbf{k}}, \quad (5)$$

with

$$\Pi_0(\mathbf{k}, \omega) = \frac{1}{L^2} \sum_{\mathbf{k}'} \frac{\vartheta(\epsilon_F - \epsilon_{\mathbf{k}'}) - \vartheta(\epsilon_F - \epsilon_{\mathbf{k}+\mathbf{k}'})}{\hbar\omega - (\epsilon_{\mathbf{k}+\mathbf{k}'} - \epsilon_{\mathbf{k}'}) + i0}. \quad (6)$$

Active branches of substrate excitations are the surface density fluctuations which consist of $2D$ electron-hole pairs and surface plasmons with dispersion law¹⁴

$$\omega_s(\mathbf{k}) = v_F k \sqrt{1 + \frac{1}{2kr_B}}, \quad r_B = \frac{\hbar^2}{me^2}, \quad k = |\mathbf{k}|.$$

The RPA spectrum of surface excitations is shown in Fig.2.

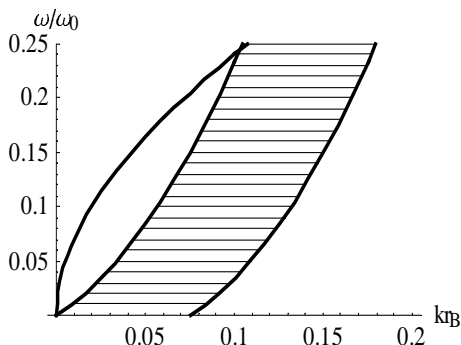


FIG. 2. Dispersion of the substrate plasmons (upper line) and quasi-continuum spectrum of electron-hole excitations, (dashed area). Frequency is measured in $\omega_0 = v_F/r_B$ units.

In the case of GaAs, the substrate parameters are $m = 0.068m_0$, m_0 is the free electron mass, $v_F = 8.2 \cdot 10^6$ cm/sec, $r_B = 0.78$ nm, $\omega_0 = v_F/r_B = 1.05 \cdot 10^{14}$ sec⁻¹. For $k < k^* \approx 0.104r_B^{-1}$, the plasmon frequency lies above the continuum spectrum of electron-hole pairs and the substrate plasmons are stable. Besides, one may easily satisfy the resonance condition for the collective plasmon mode near the stability threshold $k \sim k^*$ and QCB excitations with frequency $\omega \sim \omega^* = 2.6 \cdot 10^{13}$ sec⁻¹. For large enough $k > k^*$ the

plasmon dispersion curve lies within the quasi-continuum spectrum and plasmons become unstable with respect to decay into electron-hole pairs (Landau damping of the substrate plasmons). Dielectric losses of an isolated substrate are described by an imaginary part $\Im\epsilon_s(\mathbf{k}, \omega)$ of its dielectric function (4). This imaginary part is non-zero within the dashed region in Fig.2 due to appearance of imaginary part

$$\Im\Pi_0(\mathbf{k}, \omega) = \frac{m}{2\pi\hbar^2} \frac{1}{\kappa^2} \left[\vartheta(\kappa^2 - \nu_+^2) \sqrt{\kappa^2 - \nu_+^2} - \vartheta(\kappa^2 - \nu_-^2) \sqrt{\kappa^2 - \nu_-^2} \right],$$

$$\kappa = \frac{k}{k_F}, \quad \nu_{\pm} = \nu \pm \kappa^2/2, \quad \nu = \frac{\omega}{v_F k_F}$$

of the bare polarization operator $\Pi_0(\mathbf{k}, \omega)$ (6).

C. Interaction

Interaction between QCB and substrate is a capacitive coupling of charge fluctuations in the substrate with collective modes in the quantum wires. Assuming the distance D between the first array and the substrate to be much smaller than the distance d between arrays, one can keep only the interaction H_{s1} between the substrate and the first array. The interaction between the substrate density fluctuation at the point $\mathbf{r} \equiv (x_1, x_2)$ and the density fluctuations located in the vicinity of the point x'_1 which belongs to the n_2 -th wire of the first array is described by its amplitude $W(x_1 - x'_1, x_2 - n_2 a)$, where

$$W(\mathbf{r}) = \frac{\sqrt{2}e^2\vartheta\left(1 - \frac{|x_1|}{r_0}\right)}{\sqrt{|\mathbf{r}|^2 + D^2}}.$$

The theta function in the numerator describes the screening of Coulomb interaction within a wire or nanotube.¹⁵ In the momentum representation the interaction Hamiltonian between substrate and array has the form:

$$H_{s1} = \sqrt{\frac{\hbar}{vg}} \sum_{\mathbf{m}\mathbf{q}} W_{\mathbf{q}+\mathbf{m}} \rho_{\mathbf{q}+\mathbf{m}} \theta_{1, \mathbf{q}+\mathbf{m}}^\dagger, \quad (7)$$

where

$$W_{\mathbf{k}} = ik_1 \sqrt{\frac{vg}{\hbar a}} \int d\mathbf{r} W(\mathbf{r}) e^{i\mathbf{k}\mathbf{r}} \quad (8)$$

is proportional to a Fourier component of the interaction amplitude $W(\mathbf{r})$.

Finally, the Hamiltonian of QCB interacting with a semiconductor substrate is a sum of Hamiltonians (1), (3) and (7),

$$H = H_{QCB} + H_s + H_{s1}. \quad (9)$$

III. DIELECTRIC FUNCTION

High frequency properties of the system at zero temperature are determined by zeroes of its dielectric function

$$\frac{1}{\epsilon(\mathbf{k}, \omega)} = 1 + U_{\mathbf{k}} \Pi(\mathbf{k}, \omega). \quad (10)$$

Here

$$\Pi(\mathbf{k}, \omega) = -\frac{i}{\hbar} \int_0^{\infty} dt e^{i\omega t} \langle [\rho_{\mathbf{k}}(t), \rho_{\mathbf{k}}^{\dagger}(0)] \rangle,$$

is the polarization of the *substrate interacting with QCB*, $\rho_{\mathbf{k}}(t) = e^{iHt/\hbar} \rho_{\mathbf{k}} e^{-iHt/\hbar}$ is the density of the *substrate* electrons in the Heisenberg representation, and averaging is performed over the ground state of the Hamiltonian (9).

The Umklapp processes stimulated by the interaction between the substrate and the first array (7) as well as the interaction between arrays (2), produce modes with wave vectors $\mathbf{q} + \mathbf{m}$ with various inverse lattice vectors \mathbf{m} . This necessarily leads to appearance of non-diagonal polarization operators

$$\begin{aligned} \Pi(\mathbf{q} + \mathbf{m}, \mathbf{q} + \mathbf{m}'; \omega) &= \\ &= -\frac{i}{\hbar} \int_0^{\infty} dt e^{i\omega t} \langle [\rho_{\mathbf{q}+\mathbf{m}}(t) \rho_{\mathbf{q}+\mathbf{m}'}^{\dagger}(0)] \rangle. \end{aligned}$$

In what follows we always consider a fixed frequency ω and a fixed wave vector \mathbf{q} from the BZ. So the variables \mathbf{q} and ω are omitted below for simplicity. In the framework of RPA approach, $\Pi(\mathbf{m}, \mathbf{m}')$ satisfies the Dyson-type equation

$$\Pi(\mathbf{m}, \mathbf{m}') = \Pi_s(\mathbf{m}) \delta_{\mathbf{m}, \mathbf{m}'} + \Pi_s(\mathbf{m}) W_{\mathbf{m}} \Xi_1(m_1, \mathbf{m}'). \quad (11)$$

The first term $\Pi_s(\mathbf{m})$ in the right hand side is the substrate polarization (5) of the isolated substrate itself, $W_{\mathbf{m}} \equiv W_{\mathbf{q}+\mathbf{m}}$ is a bare vertex (8) which describes substrate - (first) array interaction, and

$$\Xi_j(m_j, \mathbf{m}') = -\frac{i}{\hbar} \int_0^{\infty} dt e^{i\omega t} \langle [\theta_{j, \mathbf{q}+\mathbf{m}_j}(t), \rho_{\mathbf{q}+\mathbf{m}'}^{\dagger}(0)] \rangle \quad (12)$$

is the correlation function of the j -th array mode and the substrate plasmon.

The Dyson equation (11) should be completed by two equations for the correlation functions (12) ($j = 1, 2$)

$$\begin{aligned} \Xi_1(m_1, \mathbf{m}') &= D_1^0(m_1) \sum_{m_2} W_{\mathbf{m}} \Pi(\mathbf{m}, \mathbf{m}') + \\ &+ D_1^0(m_1) \sum_{m_2} \Phi_{\mathbf{m}} \Xi_2(m_2, \mathbf{m}'), \end{aligned} \quad (13)$$

$$\Xi_2(m_2, \mathbf{m}') = D_2^0(m_2) \sum_{m_1} \Phi_{\mathbf{m}} \Xi_1(m_1, \mathbf{m}'). \quad (14)$$

Here $D_j^0(m_j)$ ($j = 1, 2$) is the bare correlation function of the j -th array modes

$$\begin{aligned} D_j^0(m_j) &= -\frac{i}{vg} \int_0^{\infty} dt e^{i\omega t} \langle [\theta_{j, \mathbf{q}+\mathbf{m}_j}(t), \theta_{j, \mathbf{q}+\mathbf{m}_j}^{\dagger}(0)] \rangle_0 \\ &= \frac{1}{\omega^2 - v^2(q_j + m_j)^2}, \end{aligned}$$

and another bare vertex

$$\Phi_{\mathbf{m}} = \frac{\hbar \phi}{vg} \xi_{q_1+m_1} Q \xi_{q_2+m_2} Q,$$

describes the separable inter-array interaction (2).

Solving the system of equations (11), (13) and (14) one obtains the diagonal element $\Pi(\mathbf{m}) \equiv \Pi(\mathbf{m}, \mathbf{m})$ of the polarization operator

$$[\Pi(\mathbf{m})]^{-1} = [\Pi_s(\mathbf{m})]^{-1} - |W_{\mathbf{m}}|^2 D(\mathbf{m}). \quad (15)$$

The second term on the right-hand side of this equation describes renormalization of the substrate polarization operator $\Pi_s(\mathbf{m})$ by interaction between the substrate and QCB. The factor $D(\mathbf{m})$ is a renormalized correlation function of modes of the first array

$$[D(\mathbf{m})]^{-1} = [D_1^0(m_1)]^{-1} - (w(\mathbf{m}) + \varphi(m_1)). \quad (16)$$

The first term $w(\mathbf{m})$ describes the effective interaction between the first array and substrate

$$\begin{aligned} w(\mathbf{m}) &= F(m_1) - |W_{\mathbf{m}}|^2 \Pi_s(\mathbf{m}), \\ F(m_1) &= \sum_{m_2} |W_{\mathbf{m}}|^2 \Pi_s(\mathbf{m}). \end{aligned} \quad (17)$$

The second one $\varphi(m_1)$ is the effective interaction between arrays

$$\begin{aligned} \frac{\omega_{m_1}^2}{\varphi(m_1)} &= \left[\phi^2 \sum_{m_2} \omega_{m_2}^2 D_2^0(m_2) \right]^{-1} - \Psi_{m_1}, \\ \omega_{m_j} &= v|q_j + m_j Q|, \end{aligned} \quad (18)$$

renormalized by Coulomb interaction of array modes with the substrate plasmons,

$$\Psi_{m_1} = \sum_{m'_1 \neq m_1} \frac{\omega_{m'_1}^2}{(D_1^0(m'_1))^{-1} - F(m'_1)}. \quad (19)$$

Equations (15) - (19) together with definition (10) solve the problem of dielectric properties of the combined system QCB-substrate.

The spectrum of collective excitations in QCB-substrate system is determined by zeros of the dielectric function $\epsilon(\mathbf{q}, \omega) = 0$. The key question here is the robustness of the QCB spectrum against interaction with 2D substrate excitations. Detailed analysis shows that in the long wave limit $q \ll Q$ the interaction just renormalizes the bare dispersion laws of the arrays, conserving its LL linearity. This result verifies stability of QCB plasmons with respect to substrate-QCB interaction.

The QCB-substrate interaction also results in occurrence of some special lines in the BZ. These lines correspond to resonant interaction of the substrate with the first or the second array. The resonance condition $\omega_s(\mathbf{k}) = \omega_j(\mathbf{k})$ is fulfilled along the line $LJIN$ for $j = 1$ and along the line KBM for $j = 2$ in Fig.5 below.

IV. LANDAU DAMPING

As was mentioned in subsection IIB above, dielectric losses of an isolated substrate are related to Landau damping due to decay of substrate plasmons with momentum $k > k^* \approx 0.104r_B^{-1}$ into electron-hole pair. The substrate-QCB interaction remarkably modifies the conventional picture of substrate plasmon dielectric losses. Due to QCB-substrate interaction, new domains of Landau damping appear in addition to the dashed region in Fig.2. Indeed, outside the initial instability region where $\Im\epsilon_s(\mathbf{k}, \omega) = 0$, nonzero imaginary part $\Im\epsilon(\mathbf{k}, \omega)$ (10) exists if the imaginary part of the bare polarization operator $\Im\Pi_0(\mathbf{k} + \mathbf{m}, \omega)$ differs from zero at least for one of the reciprocal lattice vectors \mathbf{m} . The main contribution to $\Im\epsilon(\mathbf{k}, \omega)$ is related to the renormalization term $w(\mathbf{m})$ in Eq.(17) due to Umklapp processes along the x_2 axis (summation over m_2 in the expression for the function $F(m_1)$ is implied). It is proportional to the fourth power of QCB - substrate interaction W^4 . The Umklapp processes along both directions $x_{1,2}$ contribute also to the renormalization term $\varphi(m_1)$ in Eq.(18). However, they contain additional small parameter ϕ^4 related to interarray interaction within QCB. These terms are not taken into account. Thus, the possible Umklapp vectors have the form $\mathbf{m}_2 = m_2 Qe_2$, $m_2 = \pm 1, \pm 2, \dots$ and in what follows we will label them by an integer number m_2 .

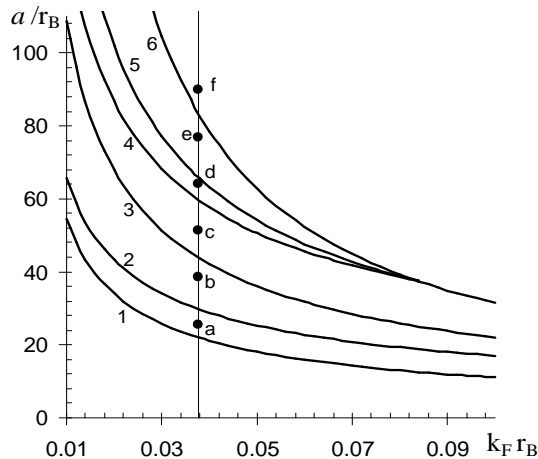


FIG. 3. Phase diagram describing appearance and structure of new regions of Landau damping. Lines 1 – 6 separate different types of new damping regions. Points $a - f$ corresponds to the structures displayed below in Figs. 4-9.

The structure of the new Landau damping regions and their existence itself is governed by interplay between the Fermi momentum of the substrate k_F and the QCB period a . The first of these parameters defines the width of the two particle excitation band (dashed region in Fig.2)

while the second determines the minimal reciprocal vector Q . In the case of sufficiently thick QCB superlattice (small a) and sufficiently low electron density within the substrate (small k_F), Umklapp processes are always ineffective because they change an initial plasmon wavevector into the outer part of the instability region. This means that only plasmons with momenta $|k| > k^*$ decay into electron-hole pairs.

Increasing the QCB period or the Fermi momentum turn the Umklapp processes effective and additional Landau damping regions appear within the circle $|k| \leq k^*$. The first factors involved are the smallest Umklapp vectors ± 1 , then new damping regions appear corresponding to the Umklapp vectors ± 2 and so on. As a result one gets a rich variety of possible damping scenarios. We describe them with the help of a “phase diagram” in the $a - k_F$ plane displayed in Fig.3 (actually dimensionless coordinates a/r_B and $k_F r_B$ are used). Here the set of curves labelled by numbers 1 – 6 separate the regions of parameters corresponding to the different Umklapp vectors and different structures of the new damping regions. There are no additional Landau damping regions below the first line. Above the sixth line Landau damping takes place within the whole circle $k \leq k^*$. Above lines with numbers $2n - 1$, the Umklapp vector $\pm n$ becomes effective. Corresponding additional damping region first has the form of a tail touching the initial Landau damping region $|k| \geq k^*$. This tail turns to the additional damping band well separated from the initial one above the line number $2n$ ($n < 3$) within some sector of directions in k -space (in what follows, these directions will be labelled by corresponding arcs of the circle).

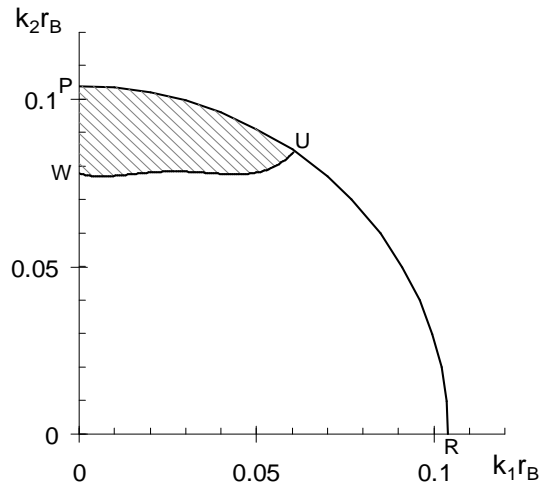


FIG. 4. New Landau damping region PUW for QCB with period $a = 20$ nm (point a in Fig.3) corresponds to the Umklapp vector -1 .

Possible structures of new damping regions corresponding to some representative points $a - f$ in the $a - k_F$ plane (see Fig.3) are displayed in detail in Figs.4-9. All these figures correspond to the $GaAs$ value of $k_F r_B \approx 0.038$. Generally speaking we should display new damping region within the whole circle $|k| \leq k^*$ in the plane k_1, k_2 . The circle center Γ is placed at the origin (we did not put the letter Γ in Figs.4-8). But

this region is always symmetric with respect to reflection $k_1 \rightarrow -k_1$ and with respect to the combined reflection $k_2 \rightarrow -k_2, m_2 \rightarrow -m_2$. This enables us to describe the damping scenarios within the quarter $k_{1,2} \geq 0$ only (complete picture of the new damping region can be easily obtained from the displayed one with the help of the reflections mentioned above).

Damping of the substrate plasmon occurs inside the arc PR in Figs.4-9 when at least one of the points in the phase space with coordinates $(\mathbf{k} + \mathbf{m}_2, \omega_s(k))$ lies within the quasi-continuum spectrum of the electron-hole excitations, whereas the “mother” point $(\mathbf{k}, \omega_s(k))$ lies above the continuum (above the dashed area in Fig.2). As was mentioned above, for small enough QCB period $a < a_1 = 17.3$ nm, the basic reciprocal lattice vector $Q\mathbf{e}_2$ is too large, the points $(\mathbf{k} + \mathbf{m}_2, \omega_s(k))$ lie outside the quasi-continuum for all m_2 and additional Landau damping region does not exist. It appears only for $a > a_1$ ($Q < 2k^* + 2k_F$). For $a_1 < a < a_2 = 23.6$ nm ($2k^* + 2k_F > Q > 2k^*$), this is the region PUW (see Fig.4) corresponding to the $m_2 = -1$ (in all Figs.4-9, the regions related to this Umklapp vector are always hatched by the hatching tilted to left). As a result, the damping tails touching the initial Landau damping region appear in certain directions of the \mathbf{k} plane.

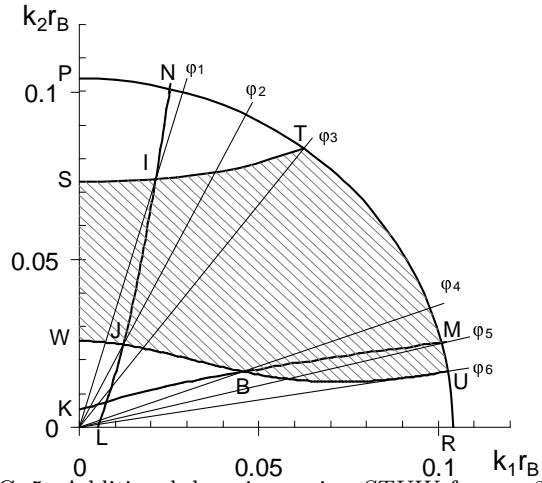


FIG. 5. Additional damping region $STUW$ for $a = 30$ nm (point b in Fig.3) corresponds to the Umklapp vector -1 and describes Landau damping tail (within the arc TU) or separate Landau band (within the arc TP). Other details of this figure are explained in the text.

For $a_2 < a < a_3 = 34.6$ nm ($2k^* > Q > k^* + k_F$), new damping region is related to the same Umklapp vector -1 , but now it has a strip-like structure bounded by the line $STUW$ in Fig.5. Note that the damping is absent within the region PTS . As a result, it is possible to divide the angle region $0 \leq \varphi \leq \pi/2$ into three sectors. Within the first one PT , $0 \leq \varphi \leq \varphi_3$, a new damping region is separated from the initial one. The second sector TU , $\varphi_3 \leq \varphi \leq \varphi_6$, corresponds to a new damping tail. Finally, within the third sector UR , $\varphi_6 \leq \varphi \leq \pi/2$, new damping region does not exist at all.

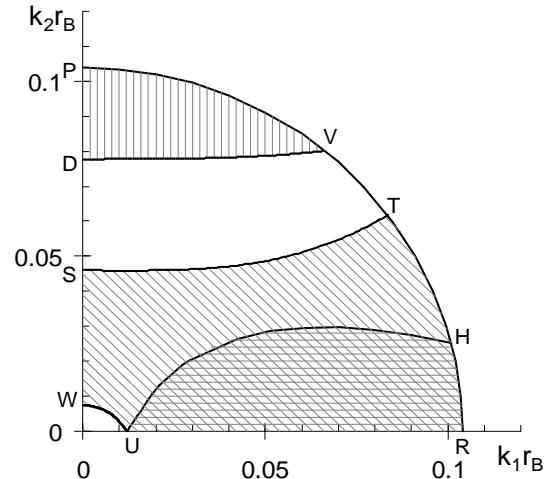


FIG. 6. In the case $a = 40$ nm (point c in Fig.3), new Landau damping regions PVD , $STRUW$, and UHR correspond to the Umklapp vectors -2 , -1 , and $+1$.

For larger QCB period, $a_3 < a < a_4 = 47.1$ nm ($k^* + k_F > Q > k^*$), the new damping regions have a more complicated structure. In fact the damping area consists of three parts (see Fig.6). The first one, $STRUW$ corresponds to the Umklapp vector -1 . Note that it is shifted to the bottom with respect to the previous case $a = 30$ nm. This part overlaps with the second part HRU . The latter corresponds to the Umklapp vector $+1$ and is hatched in Figs.6-8 by horizontal hatching. The second region PDV corresponds to the Umklapp vector -2 (in Figs.6-9 such a regions are always hatched by vertical hatching). As a result in the direction close enough to the k_2 axis, one gets a new damping band with Umklapp vector -2 and well separated new damping band with Umklapp vector -1 .

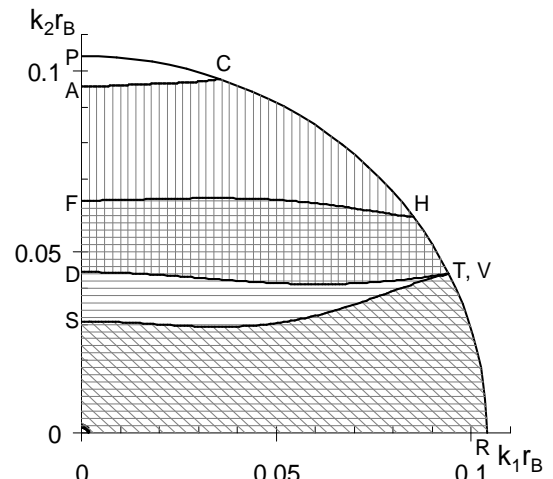


FIG. 7. New regions of Landau damping for $a = 50$ nm (point d in Fig.3). Regions $ACVD$, STR , and FHR correspond to the Umklapp vectors -2 , -1 , and $+1$

Further increase of QCB period $a_4 < a < a_5 = 52.3$ nm, $k^* > Q > 2(k^* + k_F)/3$ ($k^* \approx 2.8k_F$ for $GaAs$) leads to further extension of new damping regions. The region $ADVC$ corresponding to the Umklapp vector -2 is partially separated from the initial damping region. It

overlaps with the region $FHR\Gamma$ ($m_2 = +1$) which in its turn overlaps with the region $STR\Gamma$ ($m_2 = -1$). Actually the two latter regions do not include an extremely small vicinity of the origin Γ which is not shown in Fig.7. Visible coincidence of the points V and T in Fig.7 is an artefact of the accuracy of the figure.

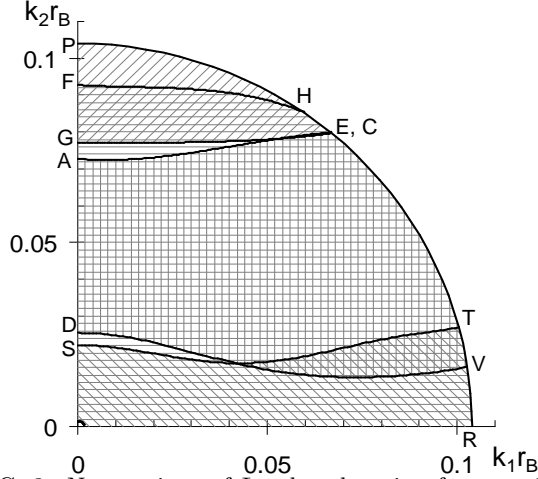


FIG. 8. New regions of Landau damping for $a = 60$ nm (point e in Fig.3). Besides the regions $ACVD$, STR , and FHR corresponding, as in the case $a = 50$ nm, to the Umklapp vectors -2 , -1 , and $+1$, new Umklapp vector -3 appears (region PEG).

Within the next interval of QCB periods $a_5 < a < a_6 = 65.2$ nm ($2(k^* + k_F)/3 > Q > 2k_F$) new damping region GPE corresponding to the Umklapp vector -3 appears. This region is hatched in Figs.8,9 by the hatching tilted to the right. Beside that the regions $ADVC$ ($m_2 = -2$), $FHR\Gamma$ ($+1$), and $STR\Gamma$ (-1) are present. As in the previous figure, visible coincidence of the points E and C in Fig.8 is an artefact of the accuracy of the figure.

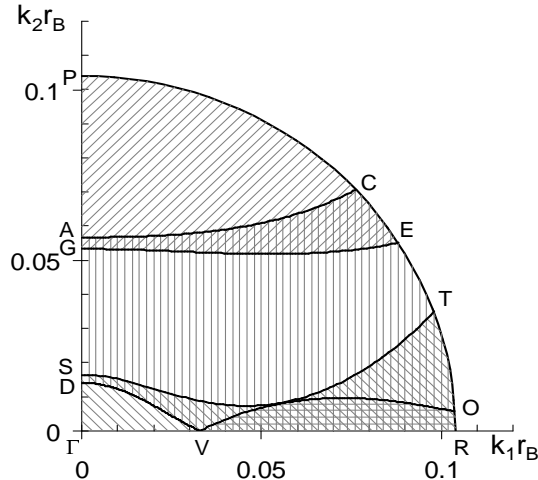


FIG. 9. The case $a = 70$ nm (point f in Fig.3). New regions of Landau damping PEG , $ACVD$, STR , whole sector GPR , and VOR correspond to the Umklapp vectors -3 , -2 , -1 , $+1$, and $+2$.

Finally for $a > a_6$ ($Q < 2k_F$), Landau damping emerges in the whole circle $|k| \leq k^*$. This occurs due

to processes with Umklapp vector $+1$. The corresponding damping region covers the whole quarter. Therefore we did not hatch it at all and used the same horizontal hatching for the new region VOR corresponding to the Umklapp vector $+2$. The region $DACRV$ is related to the Umklapp vector -2 . We emphasize that the vertex V of this region at the same time is the vertex of the region VOR , this is not an accidental approximate coincidence as in the two previous figures. The regions GPE and ΓSTR are related to the Umklapp vectors -3 and -1 correspondingly.

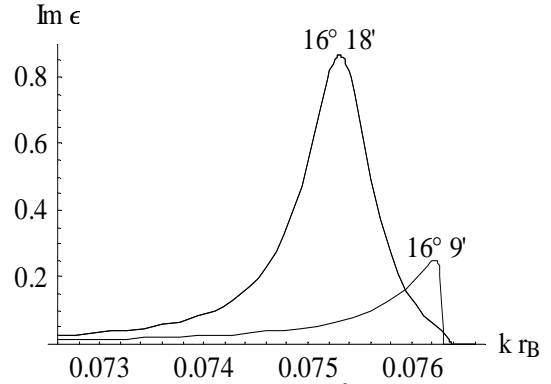


FIG. 10. Damping tail for $\varphi \approx 16^\circ$. Precursor of the resonant peak and the resonant peak are resolved quite well.

Thus, the general structure of the additional damping regions is described in Figs.4-9. However there is an additional structure of these regions. This fine structure is related to possible resonance interaction between the substrate plasmons and the QCB plasmons of the first or second array. The resonance condition for the first (second) array is written as $\omega_s(\mathbf{k}) = \omega_1(\mathbf{k})$ ($\omega_s(\mathbf{k}) = \omega_2(\mathbf{k})$).

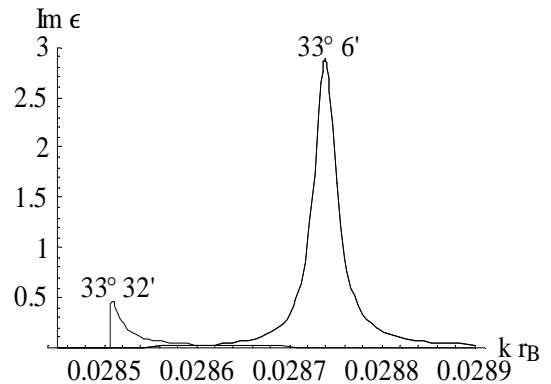


FIG. 11. Damping tail for $\varphi \approx 33^\circ$. Precursor of the resonant peak and the resonant peak are resolved quite well.

Consider such fine structure of new Landau damping region in details for QCB with period $a = 30$ nm. Here the resonance conditions are satisfied along the lines $LJIN$ and KBM (Fig.5). These lines intersect with the damping region boundaries at the points J, I, B and MB which define four rays OI, OJ, OB , and OU and four corresponding angles $\varphi_1 \approx 16^\circ 11'$, $\varphi_2 \approx 33^\circ 19'$, $\varphi_4 \approx 69^\circ$, $\varphi_5 \approx 76^\circ$. The resonance interaction takes place within two sectors $\varphi_1 < \varphi < \varphi_2$ and $\varphi_4 < \varphi < \varphi_5$.

For each $\varphi < \varphi_1$ the new damping region is a well sep-

arated damping band. The damping amplitude is small because of the small factor of order W^4 mentioned above. When $\varphi \rightarrow \varphi_1 - 0$, small peak appears near the “blue” boundary of this damping region. This peak is a precursor of the resonance between the substrate plasmon and the first array QCB plasmon (Fig.10). The same happens from the opposite side of the sector (φ_1, φ_2 when $\varphi \rightarrow \varphi_2 + 0$ (Fig.11).

Within the sector $\varphi_1 < \varphi < \varphi_2$, the damping band contains a well pronounced peak corresponding to resonant interaction between the substrate plasmon and the first array plasmons (see Figs.10,11). The peak amplitude is of order of the damping amplitude within the initial damping region. It has a Lorentz form placed on a wide and low pedestal. The peak is especially sensitive to the strength of the QCB-substrate interaction which is governed by the distance D between QCB and substrate.

To study this D dependence, let us consider the imaginary part $\Im\epsilon(\mathbf{k}, \omega)$ of the dielectric function within the considered sector $\varphi_1 < \varphi < \varphi_2$. In the vicinity of the plasmon frequency $\omega \approx \omega_s(k)$ this imaginary part is written as

$$\Im\epsilon(\mathbf{k}, \omega) = \frac{|W_{\mathbf{k}}|^2}{U_{\mathbf{k}}} \frac{-\Im w(\mathbf{k}, \omega_s(k))}{(\omega^2 - v^2 k_1^2)^2 + (\Im w(\mathbf{k}, \omega_s(k)))^2},$$

with $w(\mathbf{k}, \omega_s(k))$ being of order $|W|^2$. So the resonance peak indeed has the Lorentz like shape with height of order unity,

$$\Im\epsilon_{max} \sim \frac{|W_{\mathbf{k}}|^2}{|W_{\mathbf{k}-Qe_2}|^2} \sim 1,$$

whereas its half-width

$$\Gamma = \Im w(\mathbf{k}, v|k_1|) \sim |W_{\mathbf{k}-Qe_2}|^2,$$

is of order W^2 . The peak is displayed in Fig.12 for different values of the distance D between the substrate and the nearest (first) array. It is seen that the amplitude changes slowly with increasing distance D while its width squeezes sharply, $W^2 \sim 1/D^2$.

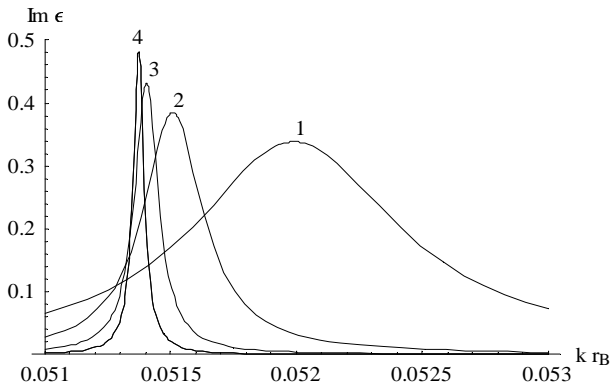


FIG. 12. Damping tail for $\varphi = 20^\circ$ for different distances D between QCB and substrate. The curves 1, 2, 3, and 4 correspond to $D = 1$ nm, 1.5 nm, 2 nm, and 2.5 nm, respectively. With increasing D , the resonant peak narrows and slowly increases, whereas the area under the curve decreases.

There is no resonance interaction within the sector $\varphi_2 < \varphi < \varphi_4$ but further increase of the angle $\varphi_4 < \varphi < \varphi_5$ leads to re-appearance of the resonant peak within the damping tail. In this case one deals with a resonance between the substrate plasmon and the QCB plasmon in the second array. Existence of this resonance is caused by inter-array interaction that brings additional small parameter to the imaginary part of the dielectric function. As a result, the width of the peak is much smaller in the second sector while surprisingly, the peak amplitude has the same order of magnitude as in the case of resonance with the first array (closest to the substrate).

Existence of the additional QCB bands (tails) of Landau damping and appearance of the resonant peaks within the bands (tails) is a clear manifestation of interplay between real $2D$ surface plasmons and quasi- $2D$ QCB plasmons.

V. CONCLUSION

In conclusion, the possibility of spectroscopic studies of the excitation spectrum of quantum crossbars interacting with semiconductor substrate is investigated. A capacitive contact between QCB and substrate does not destroy the LL character of the long wave excitations. However, quite unexpectedly, the interaction between the surface plasmons and plasmon-like excitations of QCB essentially influences the dielectric properties of the substrate. The QCB may be treated as a diffraction grid for the substrate surface, and Umklapp diffraction processes radically change the plasmon dielectric losses. Due to QCB-substrate interaction, additional Landau damping regions of the substrate plasmons appear. Their existence, form and density of losses are strongly sensitive to the QCB period. So the surface plasmons are more fragile against interaction with superlattice of quantum wires than the LL plasmons against interaction with $2D$ electron gas in a substrate.

ACKNOWLEDGMENTS

The author appreciates numerous helpful discussions with S. Gredeskul, K. Kikoin, and Y. Avishai.

-
- ¹ M.R. Diehl, S.N. Yaliraki, R.A. Beckman, M. Barahona, and J.R. Heath, *Angew. Chem. Int. Ed.* **41**, 353 (2002).
 - ² B. Q. Wei, R. Vajtai, Y. Jung, J. Ward, R. Zhang, G. Ramanath, and P. M. Ajayan, *Nature* **416**, 495 (2002).
 - ³ T. Rueckes, K. Kim, E. Joselevich, G. Y. Tseng, C. L. Cheung, and C. M. Lieber, *Science* **289**, 94 (2000).
 - ⁴ A.B. Dalton, S. Collins, E. Muñoz, J.M. Razal, V.H. Ebron, J.P. Ferraris, J.N. Coleman, B.G. Kim, and R.H. Baughman, *Nature* **423**, 703 (2003).
 - ⁵ P.W. Anderson, *Science*, **235**, 1196 (1987).

- ⁶ M. Bockrath, D.H. Cobden, J. Lu, A.G. Rinzler, R.E. Smalley, L. Balents, P.L. McEuen, Nature **397**, 598 (1999).
- ⁷ R. Egger, A. Bachtold, M.S. Fuhrer, M. Bockrath, D.H. Cobden, and P.L. McEuen, in *Interacting Electrons in Nanostructures*, p. 125, R. Haug, and H. Schoeller (Eds.), Springer (2001).
- ⁸ R. Mukhopadhyay, C.L. Kane, and T. C. Lubensky, Phys. Rev. B **63**, 081103(R) (2001).
- ⁹ I. Kuzmenko, S. Gredekskul, K. Kikoin, and Y. Avishai, Low Temp. Phys. **28**, 539 (2002) [Fiz. Nizk. Temp. **28**,752 (2002)].
- ¹⁰ S. Gredekskul, I. Kuzmenko, K. Kikoin, and Y. Avishai, Physica E **17**, 187 (2003).
- ¹¹ K. Kikoin, I. Kuzmenko, S. Gredekskul, and Y. Avishai, in *Recent Trends in Theory of Physical Phenomena in High Magnetic Fields*. Eds. I.D. Vagner, T. Maniv, and P. Wyder, NATO Sci Series, **106**, 89 (2003).
- ¹² I. Kuzmenko, S. Gredekskul, K. Kikoin, and Y. Avishai, Phys. Rev. B **67**, 115331 (2003).
- ¹³ S.G. Louie in *Carbon Nanotubes*, M.S. Dresselhaus, G. Dresselhaus, Ph. Avouris (Eds.), Topics Appl. Phys. **80**, 113 (2001), Springer, Berlin 2001.
- ¹⁴ F. Stern, Phys.Rev. Lett. **18** 546 (1967).
- ¹⁵ K. Sasaki, Phys. Rev. B **65**, 195412 (2002).